Water Resources Research

Analytical Solution of Advection-Dispersion Boundary Value Processes in Environmental Flows

Vamsi Krishna Sridharan[1,2] and Andrew M. Hein[1,2]

[1]Institute of Marine Sciences, University of California, Santa Cruz, CA, USA, [2]Fisheries Ecology Division, Southwest Fisheries Science Center, National Marine Fisheries Service, National Oceanic and Atmospheric Administration, Santa Cruz, CA, USA

Abstract The one-dimensional advection-dispersion equation with streamwise boundaries has been used to model a wide range of real-world processes including groundwater contaminant transport, atmospheric plume deposition, and the movement of planktonic organisms and migratory animals through riverine systems. Imposing boundary conditions at upstream and downstream locations complicates the analysis of this equation, and processes that require such boundary conditions are, therefore, typically modeled using approximations that are valid only under certain conditions. Approximations typically involve a simplification of the mass influx into the system, require a large separation between source and boundary, or work only in either strongly advection- or strongly dispersion-dominated systems. Here, we circumvent these limitations by providing an analytical solution to a class of advection-dispersion equations that are broadly applicable to the processes described above as well as many other physical and biological problems. Our solution makes it possible to relax the assumptions required under previous analytic approximations, making it a more flexible approach for modeling advection-dispersion processes under realistic field conditions. We show that the solution is in good agreement with random walk simulations. To illustrate the broad utility of the method, we also apply it to an empirical data set from a population of migratory fish moving through a river system in the California Central Valley and demonstrate that it describes the data more accurately than do existing methods.

1. Introduction

One-dimensional advection-dispersion (1-D-AD) processes are ubiquitous in fluid systems. A nonexhaustive listing of such examples includes (i) the movement of contaminants in surface water systems and the formation of a concentration boundary such as an estuarine turbidity maximum (e.g., Schoellhamer, 2000), (ii) the movement of a tracer in groundwater toward a water body or obstruction (e.g., Golz & Dorroh, 2001), (iii) thermal exchange processes by conduction and convection in porous media flow (e.g., Kurylyk & Irvine, 2016; Luce et al., 2013), (iv) the absorption of dispersing atmospheric plumes on the ground or other surfaces (e.g., Ermak, 1977; Lin & Hildemann, 1997), (v) biological dispersal processes (e.g., Okubo & Levin, 1989), (vi) the evolution of chaotic dynamical systems within a coherent part of the system domain (Wilkinson et al., 2010), and (vii) the study of the migration of fish through river systems (e.g., Zabel & Anderson, 1997) (see Table 1 for additional examples).

We subsequently outline the 1-D-AD equation with constant coefficients for a domain with a boundary that is either fully reflecting, fully or partially absorbing, or seeding (i.e., mass is introduced into the system at the boundary) in section 2 and present a general solution in section 3. This solution may be applied to the movement of any quantity such as thermal energy, suspended sediments or the concentration of a solute in water, or the number of dispersing organisms (e.g., plankton and migratory fish) present in a given length of river. Our solution is exact throughout the spatial domain and for all times and for all the possible Péclet number (Pe) regimes, although the integral appearing in the solution must be evaluated numerically. Here, $\text{Pe} = \frac{u x_B}{K}$, the ratio of the dispersive time scale, $\frac{x_B^2}{K}$, to the advective time scale, $\frac{x_B}{u}$, for a system of length x_B with dimension (L), with a mean velocity u with dimension (LT^{-1}), and a dispersion coefficient K with dimension $(L^2\ T^{-1})$. Earlier solutions to the advection-dispersion problem with such boundaries (e.g., Ermak, 1977; Grant & Wilkinson, 2015; Lin & Hildemann, 1996, 1997; van Genutchen & Alves, 1982) were approximate and, as we illustrate

Table 1
Applications of the One-Dimensional Advection-Dispersion Equation With Different Types of Boundary Conditions in Various Fields

Field	Reflecting boundary	Absorbing boundary	Seeding boundary	Partially absorbing boundary
Surface water transport and mixing	Estuarine turbidity maximum (Schoellhamer, 2001)	Absorption of heat in cold-water pools in river networks (Monismith et al., 2009)	Sediment resuspension (Lee et al., 2002)	Sediment deposition with resuspension (Lee et al., 2002)
Porous media flow	Groundwater flow toward impermeable barriers (LaBolle et al., 1998)	Tracer studies at extraction wells (Golz & Dorroh, 2001)	Seepages from different porosity layers in groundwater flow (Berkowitz, 2002)	Sorption of organic matter in groundwater (Roberts et al., 1982)
Multiphase thermal exchange	Convection near surfaces (Szymczak & Ladd, 2003)	Heat exchange with streambed (Luce et al., 2013)	Heat exchange with atmosphere in streams (Luce et al., 2013)	Coupled groundwater and streamflow thermal exchange (Kurylyk & Irvine, 2016)
Atmospheric plumes	Inversion layers (Stockie, 2011)	Absorption at the ground (Stockie, 2011)	Reentry of pollutants through terrestrial boundary layers (Loeck et al., 2018)	Dry deposition (Lin & Hildemann, 1997)
Biological dispersal	End of suitable habitat ranges for aquatic animals (Speirs & Gurney, 2001)	Transition to region of no return in rivers for aquatic animals (Speirs & Gurney, 2001)	Pollen resuspension near the ground (Okubo & Levin, 1989)	Pollen settling (Okubo & Levin, 1989)
Fisheries	Open water tagged fish distributions near land (Sibert et al., 1999)	Mark-recapture studies in rivers (Zabel & Anderson, 1997)	Models of habitat use in which some fish are allowed to enter a domain (Gurney et al., 2001)	Fish screens near water diversion facilities (Kimmerer, 2008)

here, yield inaccurate estimates of the spatial density of incipient mass in large regions of the spatial domain and for systems in which the advection and dispersion are equally important.

In the past, several approximate analytical solutions have been formulated, but these apply only to a small region of the system domain and only for very small or large Péclet numbers (Grant & Wilkinson, 2015; Rubbab et al., 2016). Existing solution methods typically involve either (i) only radiating boundary conditions, which allow the unaffected passage of the quantity being transported, with analysis based on eigenfunction expansions and separation of variables (e.g., Golz & Dorroh, 2001; Smith, 1983) or Laplace transforms (Brenner, 1962; Danckwerts, 1953; van Genutchen & Alves, 1982), or (ii) simplifying assumptions about the flux at the boundaries that lead to approximate solutions (Ermak, 1977). The standard flux approximations (e.g., Ermak, 1977; Grant & Wilkinson, 2015) are only applicable for boundaries that are far away from the source, or equivalently, for times very close to the actual release and for systems with large Péclet number. An alternate class of solutions employs the Green's function obtained by solving an adjoint equation with the relevant boundary conditions (Lin & Hildemann, 1996, 1997; Yeh, 1975). However, even in these more generally applicable solutions, the implicit assumption is that the advective flux toward the boundary is negligible (i.e., a small Pe approximation) except very close to the boundary (e.g., Lin & Hildemann, 1996). As a direct consequence of the approximations of (i) large source-boundary separation, (ii) times close to the onset of the release, (iii) very large or very small Péclet number regimes, or (iv) negligible advection in the bulk of the domain, the intuition built by these solutions is that the absorbing boundary merely modifies the flux due to the free passage of the incipient mass. In what follows, we illustrate that this is not necessarily the case.

In our solution, we adopt a method based on continuously modified images in which, at each infinitesimal time, the density moving toward (or away from) the boundary is modified by its current mirror image (Figure 1). We outline this method in section 3.1. Our solution is attractive because it provides a fast, analytical alternative to more expensive numerical methods such as particle tracking models (Dimou & Adams, 1993) or finite volume solvers (Lazarov et al., 1996) in cases when the dynamics of the system are reasonably spatially uniform and temporally stationary. In addition, neither solutions by eigenfunction expansions (e.g., Golz & Dorroh, 2001; Smith, 1983) nor random walk simulations for nonradiating boundaries (e.g., Grant & Wilkinson, 2015) provide intuition of the physical processes occurring near the boundary, whereas our method addresses the boundary process directly.

In sections 3.2 and 4.1, we use random walk simulations to show that our solution performs favorably in comparison with a typical approximation given by Grant and Wilkinson (2015). As a concrete example of the generality of our method, in sections 3.3 and 4.2, we use it to analyze an empirical data set describing the movements of migratory fish through an estuary system in California. The 1-D-AD process is regularly used as a continuum model (e.g., McKenzie et al., 2009; Moorcroft & Lewis, 2006) to describe the movements of animals, where each animal's motion is assumed to follow a random walk with bias. In particular, in studying the movements of migratory fish in rivers, fish are often tagged and released at some location, and then subsequently, their passage is
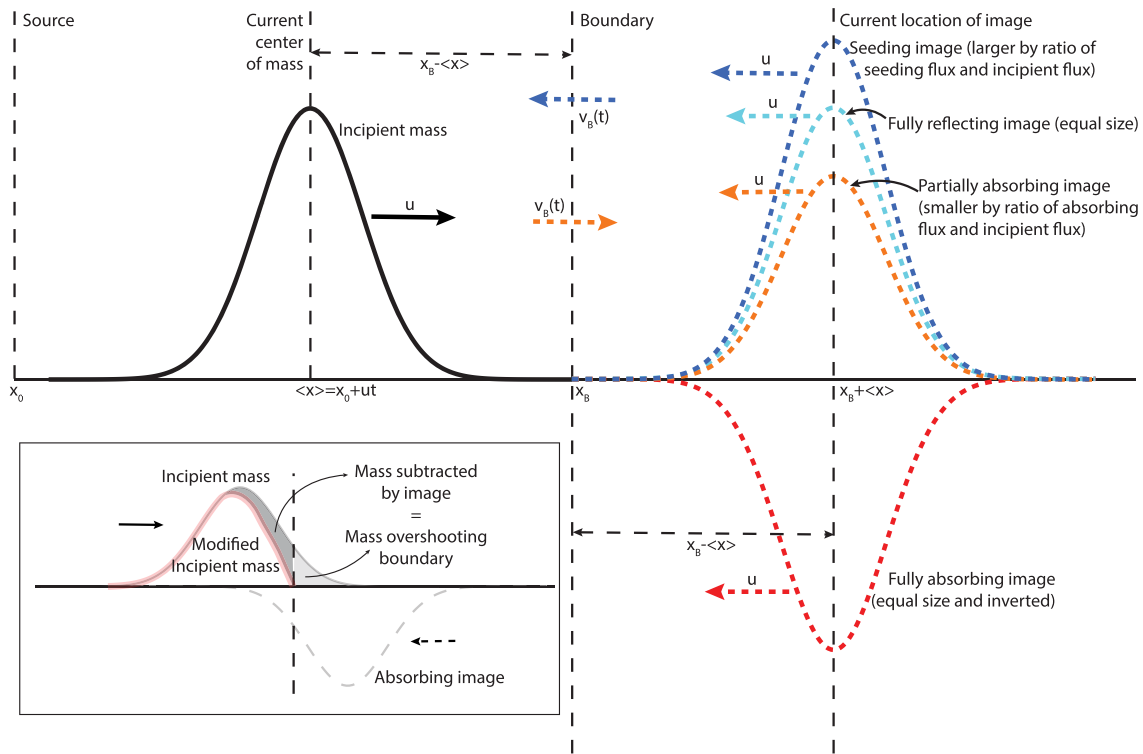
Figure 1. Schematic of the solution by the method of images. For a pulse release of mass located at x_0, the incipient density (solid black line) advects and disperses over to a new position $x = x_0 + ut$ while continuously being modified by the effects of a mirror image which is located at the reflection of x with respect to the boundary (dashed colored lines) and is advecting toward the boundary (colored arrows near the mirror images). The type of mirror image depends on the boundary conditions, and its size relative to the incipient density is given by equation (4c). The fully reflecting boundary has a flux of zero at the boundary, while the fully absorbing boundary has a density of zero at the boundary. The seeding and partially absorbing boundaries have specified boundary fluxes (colored arrows at the boundary). In the inset, an example of the modification of the incipient density (gray line) by the image (dashed gray line) and the resulting density (thick pink line) due to the removal of mass that has left the domain (light shaded area) by the negative mass added by the image source (dark shaded area) is shown for the case of the absorbing boundary.

recorded at a downstream location. The 1-D-AD equation has been used to model these movements and infer movement parameters (e.g., Zabel & Anderson, 1997). We illustrate that our solution is able to recover the observed spread as well as the peak in arrival rates of tagged fish at a downstream detection station, while a free-boundary approximation introduces unrealistically large flux across the boundary and dispersion. The application of our solution method to fish movement illustrates the value of incorporating the correct boundary conditions in these types of problems in a general solution framework. This problem also allows us to demonstrate the application of our solution in general to animal movement problems in environmental flows.

2. The 1-D-AD Equation

The most general form of the 1-D-AD equation with constant coefficients is given by (Fischer et al., 1979)

$$\frac{\partial C}{\partial t} + u \frac{\partial C}{\partial x} = K \frac{\partial^2 C}{\partial x^2}, \qquad (1)$$

where C is the density of some quantity described at a location, x, downstream of the origin at any time, t, u is the along-stream drift velocity with which the spatial density moves, and K is the effective along-stream dispersion coefficient which represents processes that deform and dilate the spatial density. Despite its simplicity, equation (1) is still widely used in the study of physical (e.g., Banas et al., 2004) and biological (e.g., Visser, 1997) surface water transport and mixing processes. It is also used to study animal movement patterns (e.g., Moorcroft & Lewis, 2006; Zabel & Anderson, 1997), where it provides a simple modeling

framework that can be sufficient under certain conditions (e.g., Moorcroft & Lewis, 2006) or a benchmark that can be used to interpret the output of more complex analyses using methods such as particle tracking models (e.g., Sridharan, 2015).

The processes represented by u and K depend on the application. In the case of estuarine transport and fate, they are hydrodynamic processes that, respectively, represent the transport and some gradient-driven mixing processes such as shear flow dispersion, tidal trapping, gravitational circulation, and chaotic tidal mixing (e.g., Fischer et al., 1979). In groundwater remediation, they represent the mean flow and diffusion of contaminants (e.g., Roberts et al., 1982). In particle physics, they represent the ensemble mean drift and random diffusive movements of many particles (Risken, 1996). In the case of populations of fish in rivers, they represent the average movement of the group and the rate of dispersal of the fish. We note that as written with constant u and K, the simplified system in equation (1) does not capture unsteady and nonuniform drift and dispersion, rate kinetics, and other sources and sinks. Such complications can be handled by suitable variable transformations (e.g., Bennett, 1971; Golz & Dorroh, 2001; Smith, 1983).

For the cases of interest here, equation (1) is subject to the initial condition that $C(x,0) = f(x)$. For an initial mass flux, $\dot{m}(x, 0)$, entering the system over an infinitesimal duration, Δt, we approximate $C_\xi(x,0)$, the contribution to $C(x,0)$ due to the mass influx at a spatial location ξ, with a narrow Gaussian, $\frac{\dot{m}(\xi, 0)\Delta t}{\sqrt{4\pi K \Delta t}} e^{-\frac{(x-\xi)^2}{4K\Delta t}}$.

The simple radiating boundary condition at the origin, over an infinitesimal distance Δx in which the concentration may be assumed to be uniform, is

$$uC(0, t) - K\frac{\partial C}{\partial x}\bigg|_{(0,t)} = \frac{\partial C(0, t)}{\partial x} \Delta x \tag{2}$$

We must impose a second boundary condition at x_B. Various boundary types are possible depending on the physical conditions being modeled. We have provided several examples from various fields in Table 1. For a fully reflecting boundary, we have a Neumann boundary condition (Lin & Hildemann, 1997)

$$\frac{dC}{dx}\bigg|_{(x_B,t)} = 0. \tag{3a}$$

This boundary condition can be represented by an image source of identical configuration to the original density at any given time (Figure 1). On the other hand, for a fully absorbing boundary, the Dirichlet boundary condition is (Lin & Hildemann, 1997)

$$C(x_B, t) = 0. \tag{3b}$$

This can be represented by an image source of identical oppositely signed configuration to the original density at any given time (Figure 1). For a partially absorbing or seeding boundary (Golz & Dorroh, 2001; Lin & Hildemann, 1997), the Robin boundary condition is

$$\frac{\partial C}{\partial t} + uC(x_B, t) - K\frac{\partial C}{\partial x}\bigg|_{(x_B,t)} = v_B(t)C(x_B, t). \tag{3c}$$

To see that this is indeed a Robin boundary condition, we can simply set $\mathscr{G}(t) = v_B(t)C(x_B, t) - \frac{\partial C}{\partial t}$ on the right-hand side. This condition seeds mass when the settling velocity, v_B, is negative. The boundary absorbs mass when v_B is positive. Such boundaries may be represented by an image source of identical configuration to the original density with strength $\alpha = 1 + \frac{|v_B(t)|C(x_B,t)}{uC(x_B,t) - K\frac{\partial C}{\partial x}\big|_{(x_B,t)}}$ when seeding and $1 - \frac{|v_B(t)|C(x_B,t)}{uC(x_B,t) - K\frac{\partial C}{\partial x}\big|_{(x_B,t)}}$ when absorbing and at any given time (Figure 1). The rationale for this formulation is that the ratio of the boundary condition induced flux to the radiating flux at the boundary sets the additional strength of the mirror image needed to achieve the overall flux balance at any given time. We note that at steady state, equation (3c) encompasses the cases of free passage if $v_B(t) = 0$, the fully reflecting boundary if u and $v_B(t)$ are both zero, and the absorbing boundary if $C(x_B, t) = 0$. This formulation becomes very useful subsequently in section 3.1.

3. Solution and Validation of the 1-D-AD Equation

We subsequently develop a solution to the system of equations (1) to (3) using the method of images in which an image source is continuously modified. We discuss the formulation of this solution and its comparison with numerical simulations, existing approximate solutions, and real data below.

3.1. Analytical Solution by the Method of Images

Consider the 1-D-AD equation given in equation (1). The density at any t is simply the sum over space of the modifications of the density at time $t - \Delta t$ located in an infinitesimal interval $d\xi$ centered at ξ by a Green's function given by $\frac{1}{\sqrt{4\pi K \Delta t}} e^{-\frac{(x-\xi-u\Delta t)^2}{4K\Delta t}}$ moving with the drift velocity, u. This Green's function is the standard impulse response for a 1-D-AD process and may be obtained by making a self-similar variable transformation to $\eta = \frac{x - ut}{\sqrt{4Kt}}$ that converts equation (1) into an ordinary differential equation that may be easily solved using a Fourier transform (see, e.g., Fischer et al., 1979). Implicit in the spatial density structure is the image source corresponding to the type of boundary condition at x_B. In its most general form, the solution for the density is (Fischer et al., 1979)

$$C(x,t) = \int_{-\infty}^{x_B} g(\xi, t-\Delta t) \frac{d\xi}{\sqrt{4\pi K \Delta t}} e^{-\frac{(x-\xi-u\Delta t)^2}{4K\Delta t}}, \tag{4a}$$

where

$$g(\xi, t-\Delta t) = \underbrace{C(\xi, t-\Delta t)}_{\text{Source}} + \underbrace{\alpha C(2x_B - u(t-\Delta t) - \xi, t-\Delta t)}_{\text{Image}} + \underbrace{\frac{\dot{m}(t-\Delta t)\Delta t}{\Delta x}}_{\text{Influx}}. \tag{4b}$$

The various boundary conditions may be represented by varying α as

$$\alpha = \begin{cases} 0 \; ; & \text{Free passage or radiating} \\ 1 \; ; & \text{Fully reflecting} \\ -1 \; ; & \text{Fully absorbing} \\ 1 - \dfrac{v_B\{tC\{x_B t}{uC\{x_B t - K\dfrac{\partial C}{\partial x}\Big|_{x_B t}} ; & \text{Seeding or partially absorbing.} \end{cases} \tag{4c}$$

Here, $g(\xi, t - \Delta t)$ is the density at a spatial location ξ which includes the effect of the image source. The recurrent form of equation (4b) ensures that the effect of the advecting image over time is fully accounted for. In practice, we replace the integration at each time step in equation (4a) by a summation in which $d\xi = \Delta x$. To reduce the numerical error when performing this summation, we estimate the spatial derivative in α using second-order backward differencing (equation (A2) in Appendix A). We note that our solution in exact, because we only resort to numerically integrating equation (4a), and do not discretize equation (1).

3.2. Numerical Simulations

We performed a series of numerical simulations to test our solution given in equation (4). These were simple 1-D random walks given by (Visser, 1997)

$$x_p(n+1) = x_p(n) + u(n)\Delta t + R\sqrt{2K\Delta t}, \tag{5}$$

where $R \in N(0,1)$ is a standard normally random number and we use a Forward Euler time marching scheme to update the pth particle's position, x_p, at time step n. Equation (5) produces a free-passage numerical solution unless the behavior of the walker is modified. For example, a fully reflecting boundary can be achieved by reflecting those particles that have overshot the boundary by (Szymczak & Ladd, 2003) $x_p'(n+1) - x_B$ as

$$x_p(n+1) = 2x_B - x'_p(n+1). \tag{6a}$$

A solution with an absorbing boundary is achieved simply by removing particles that arrive at x_B at each time step. A solution with a seeding boundary reflects those particles that have overshot the boundary by $x'_p(n+1) - x_B$ as in the case of the reflecting boundary and, in addition for $N(x \geq x_B)$ particles that have overshot the boundary, seeds approximately

$$2\frac{v_B(t)\Delta t}{\Delta x}N(x \geq x_B), \tag{6b}$$

new particles into the domain at a location given by (see Appendix A)

$$x_p(n+1) = x_B + v_B(t)\Delta t. \tag{6c}$$

A solution with a partially absorbing boundary loses mass at a rate of (see Appendix A)

$$2\frac{v_B(t)\Delta t}{\Delta x}N(x \geq x_B). \tag{6d}$$

To compare the numerical simulation to analytical solutions, we released $N = 100{,}000$ particles at the origin at a rate of $\dot{m}(t) = \begin{cases} N; t = 0 \\ 0; t>0 \end{cases}$ and simulated their movement over 100 km with and $\Delta t = 100$ s in the free-passage simulation. We binned the resulting particle positions into $\Delta x = 100$ m width neighborhoods. In the simulations with a boundary, we located the boundary at 50 km downstream of the origin. We advected the particles at a velocity of 0.5 m/s and set the dispersion coefficient at 100 m^2/s. When the boundary was seeding or partially absorbing, we set $|v_B| = 0.1$ and 0.3 m/s to show the qualitative difference between the two cases.

To test the performance of our solution, we compared it with a typical approximate solution. Such a solution in which the absorbing boundary is approximated as a modification of the flux of arriving particles (the first term on the right-hand side of equation (7)), by antiparticles located at the boundary (the second term on the right-hand side of equation (7)), was given by Grant and Wilkinson (2015) as

$$C(x,t) = \underbrace{\int_0^t \frac{\dot{m}(t)}{\sqrt{4\pi K(t-\tau)}}e^{-\frac{[x-x_B-u(t-\tau)]^2}{4K(t-\tau)}}\,d\tau}_{\text{Incipient mass flux at the boundary}} - \tag{7}$$

$$\int_0^t \underbrace{\left[\frac{1}{\sqrt{4\pi K\tau^3}}e^{-\frac{(x_B-u\tau)^2}{4K\tau}}\right]}_{\text{Antiparticle arrival}} \underbrace{\frac{1}{\sqrt{4\pi K(t-\tau)}}e^{-\frac{[x-x_B-u(t-\tau)]^2}{4K(t-\tau)}}\,d\tau.}_{}$$
$$\underbrace{\phantom{\int_0^t \left[\frac{1}{\sqrt{4\pi K\tau^3}}e^{-\frac{(x_B-u\tau)^2}{4K\tau}}\right]\frac{1}{\sqrt{4\pi K(t-\tau)}}e^{-\frac{[x-x_B-u(t-\tau)]^2}{4K(t-\tau)}}\,d\tau}}_{\text{Antiparticle flux annihilating the incipient mass}}$$

We discuss this comparison in section 4.1.

3.3. Comparison With Animal Movement Data From Migrating Fish

To test the utility of equation (4) in describing empirical processes in riverine and estuarine systems, we used our solution to model the arrivals at a downstream hydrophone station of acoustically tagged fish released at a riverine location in the Sacramento-San Joaquin Delta system in California. The Delta is an inverted fan estuary that is driven at its landward end by freshwater inflow from the Sacramento and San Joaquin Rivers (Figure 2; Monismith et al., 2009; Moyle et al., 2010). The seaward end of the Delta drains into the Pacific Ocean through San Francisco Bay. A detailed description of the hydrodynamics of this system may be found in Sridharan et al. (2018).
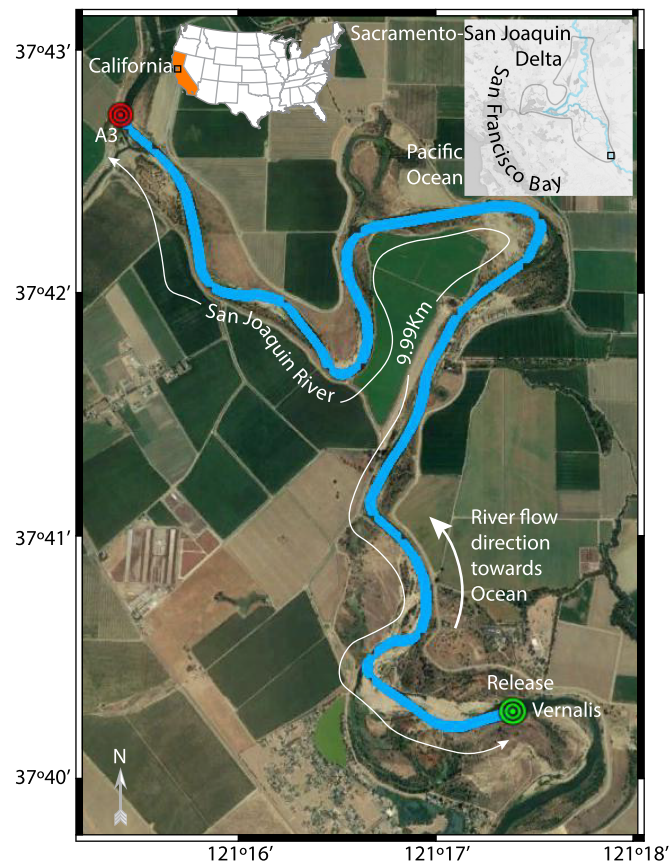
Figure 2. The release location and detection Station A3 along the San Joaquin River in 2011. The insets show the state of California and the Sacramento-San Joaquin Delta (gray boundary) which connects to San Francisco Bay and the Pacific Ocean. The Sacramento (North) and San Joaquin (South) Rivers (blue lines) are indicated in the San Francisco Bay-Delta inset.

The data set considered here consists of the migratory movements of a population of steelhead trout, a species of fish native to California. Juvenile steelheads migrate through the Delta to mature in the Pacific Ocean (McEwan, 2001). To understand their migration patterns, studies were conducted in which fish were implanted with miniature transmitters that produce an acoustic signal. These signals are received at hydrophones located at various stations positioned throughout the Delta. This system allows one to determine when each fish arrives at a particular location in the system where a hydrophone is located. Here, we focus on a large fish release that occurred in 2011. In this experiment, fish were tagged and released at Vernalis, a city on the San Joaquin River (Figure 2), and their first arrival times were recorded at various downstream stations. In Figure 2, we indicate the location of one such station (San Joaquin River Group Authority, 2013). Because only the first detections of fish at a hydrophone are typically retained, this is an example of the fully absorbing boundary at each detection station (Bailey, 1952). Here, we discuss the first arrivals of fish at A3 station, which is located 9.99 km downstream of Vernalis (Figure 2). We chose a station relatively close to the release site because at such short distances, the typical boundary flux and free-passage approximations break down. In this year, there were 1,103 fish released between March 22 and June 18 in five release groups (San Joaquin River Group Authority, 2013).

As a point of comparison, we also checked the solution of equation (4) against the free-passage solution given by (Fischer et al., 1979)

$$C(x,t) = \int_0^t \frac{\dot{m}(\tau)}{\sqrt{4\pi K(t-\tau)}} e^{-\frac{[x-u(t-\tau)]^2}{4K(t-\tau)}} d\tau. \tag{8}$$

To perform this comparison, we set the optimal values for u and K for each release group as (Fischer et al., 1979)

$$u = \frac{x_B}{\bar{t}} \quad K = \frac{1}{2}\frac{d\sigma_x^2}{d\bar{t}} = \frac{1}{2}u^2\left(\frac{\sigma_{t,x_B}^2 - \sigma_{t,o}^2}{\bar{t}}\right) \quad \bar{t} = \frac{1}{N}\sum_{i=1}^{N}\left(t_{i,x_B} - t_{i,0}\right) \qquad . \tag{9}$$

Here, we obtained the spatial cloud size, σ_x^2, from the temporal cloud size σ_t^2 by assuming that the mean velocity is constant in space and time.

As a measure of goodness of fit, we used the Kulback-Leibler divergence between the recorded and estimated densities of fish just near A3 station as (Csiszár, 2003)

$$D_{KL}[N_{\text{Solution}}(t)\|N_{\text{Data}}(t)] = \int_0^t N_{\text{Solution}}(\tau)\ln\left[\frac{N_{\text{Solution}}(\tau)}{N_{\text{Data}}(\tau)}\right]d\tau. \tag{10}$$

Here, $N_{\text{Data}}(t)$ is the total number of tagged fish detected in each day at Station A3. $N_{\text{Solution} \in \{(4) \text{ or } (8)\}}(t)$ is given by integrating the estimated rate of passage of fish across the location of Station A3 over each time step using either equation (4) or (8) (adapted from Zabel & Anderson, 1997, for a continuous release)

$$N_{\text{Solution}}(t) = N_{\text{Cumulative}}(t)\int_{t_i}^{t_{i+1}} F_{\text{Solution}}(\tau)d\tau$$

$$F_{\text{Solution}}(t) = -\frac{1}{N_{\text{Cumulative}}}\frac{d}{dt}\left[\int_{-\infty}^{x_B} C_{\text{Solution}}[\xi,\tau]d\xi\right] \qquad , \tag{11}$$

$$N_{\text{Cumulative}}(t) = \sum_{i=0}^{R_t} N_i; t = R_t\Delta t$$

where $F_{\text{Solution}}(t)$ is the estimated flux of fish across the detector at time t and $N_{\text{Cumulative}}(t)$ is the cumulative number of fish that have been detected over R_t time steps till time t, the spatial and temporal integrations are performed using the trapezoidal rule, and the temporal derivate is obtained by central differencing. Equation (11) establishes the equivalence between the estimated density and number of fish being detected. Equation (10) measures the information lost when $N_{\text{Solution} \in \{(4) \text{ or } (8)\}}$, the daily sum of estimated number of fish detections from equations (4) or (8), is used to approximate the observed flux of individuals (Burnham & Anderson, 2002). We calculated the predicted density using equations (4) or (8) with dt=100 s and Δx=100 m.

4. Results

We demonstrate the value of the solution in equation (4) by comparing it with numerical simulations as well as a commonly used approximate solution. In these comparisons, we show that our solution outperforms the approximations of equations (7) and (8).

4.1. Validation With Random Walk Models

In a comparison between the solutions of equations (4) and (7) for an absorbing boundary condition, we observe that equation (4) is able to recover the numerical solution closely for all times (Figure 3). This is because the mirror image ensures that the incipient density is itself modified continuously according to the loss of mass at the boundary. Equation (4) is also able to match the numerical simulation results for the four different boundary types we discussed in section 2 (Figure 4).

The error in estimating the density over the entire domain at any time, t, given by

$$\varepsilon_T(t) = \left[\frac{N_{\text{Cumulative}}(t) - \int_{-\infty}^{x_B} C(x,t)dx}{N_{\text{Cumulative}}(t)}\right]\times 100, \tag{12a}$$

is typically lower than 6%. The error in the density estimation at the boundary, given by

$$\varepsilon_B(t) = \left[\frac{N_{[x_B-\Delta x, x_B]}(t) - C(x_B,t)\Delta x}{N_{[x_B-\Delta x, x_B]}}(t)\right]\times 100, \tag{12b}$$
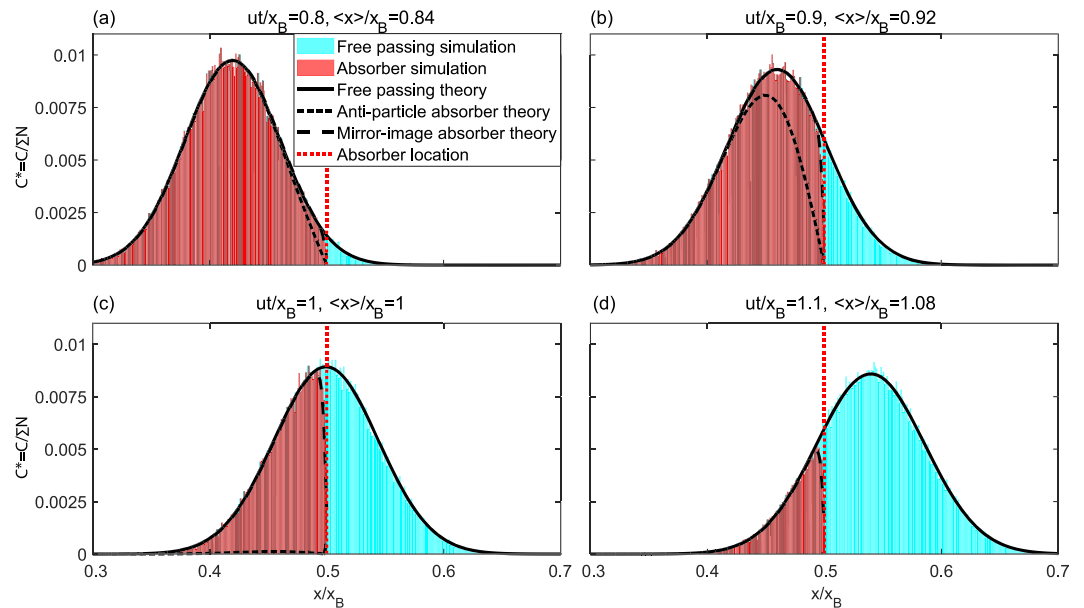
Figure 3. Comparison of numerical results with analytical solutions of an absorbing boundary condition for different times (a–d). The mirror-image solution method of equation (4) outperforms the approximate solutions of equations (7) and (8) at all times. In (a)–(d), x indicates the location of the center of mass of the freely passing cloud of particles. The integration in equation (4a) is performed using the trapezoidal rule. Note that when estimating the flux of mass across the boundary, at each time step, the free-passage assumption results in slightly higher mass than the absorbing boundary representation (the difference in area between the solid black line, the dashed black line, and the dotted red line). When equation (8) is used to estimate the flux of mass across the boundary, this error accumulates over time.
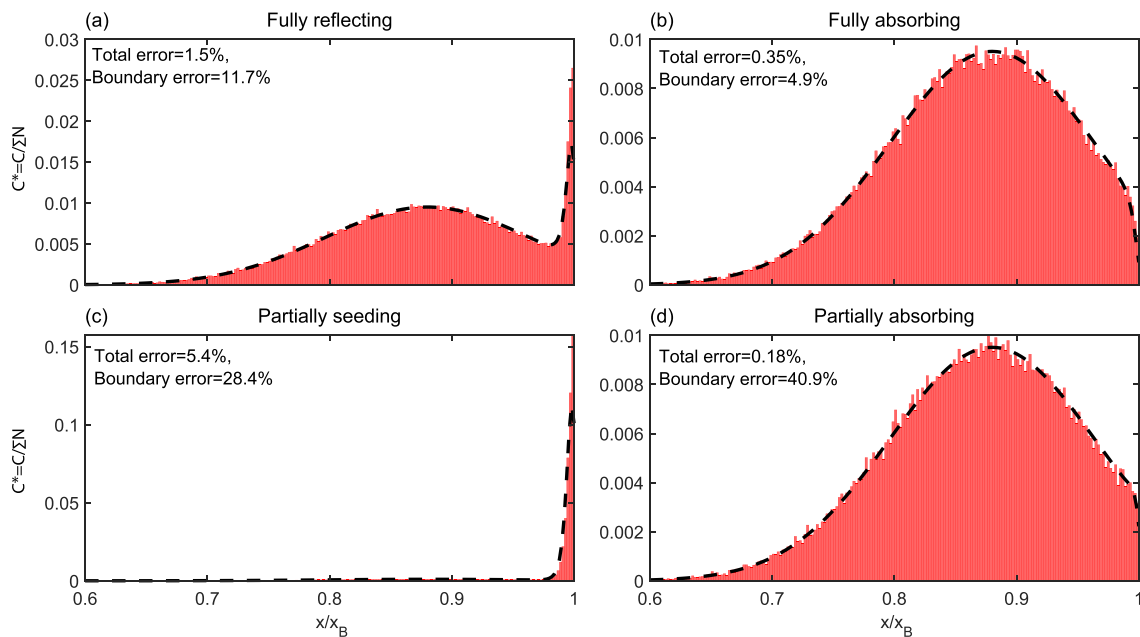

Figure 4. Numerical solution (histogram) versus solution by the method of images equation (4) (dashed line) for (a) fully reflecting, (b) fully absorbing, (c) partially seeding, and (d) partially absorbing boundary conditions, at $\frac{ut}{x} = 0.44$. The discrepancies between the simulations and equation (4) in (c) and (d) are due to the number of particles simulated, the binning of the histograms, and the finite difference approximations of the derivative in equation (A2) in Appendix A. The integration in equation (4a) is performed using the trapezoidal rule.
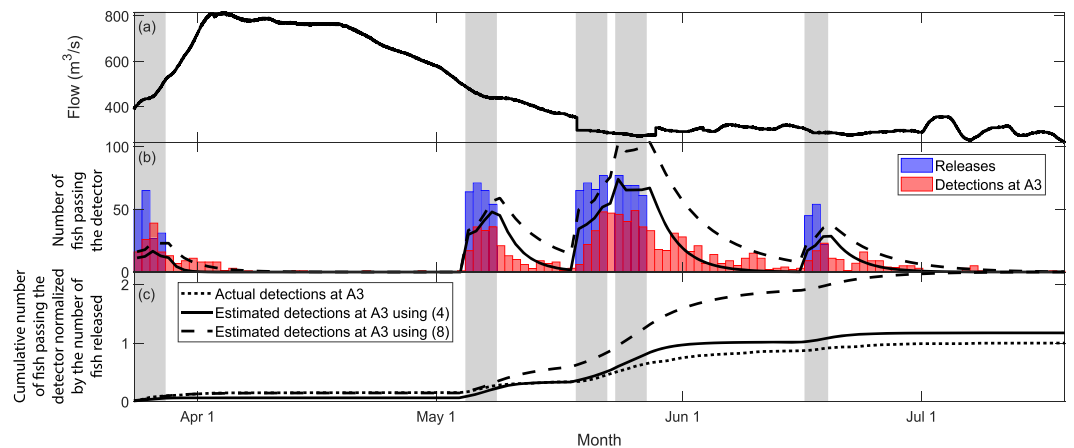
Figure 5. Comparison of the fish detections at a location downstream of the release site (equations (4) and (8)). In (a), the instantaneous flow at a location near the release site (Vernalis, CA) is shown. In (b), the releases, detections, and solutions have been binned into daily intervals for clarity. In (c), the cumulative densities normalized by the number of fish released are shown. The double counting in the free-passage solution is particularly severe at this station. Gray regions indicate release durations. Shaded bars indicate release periods. The optimal parameter values and comparative metrics $(u, K, D_{KL,(5)}, D_{KL,(8)})$ for the five release groups are (0.03 m/s, 457 m^2/s, 0.3, 1), (0.017 m/s, 154 m^2/s, 0.5, 2.4), (0.019 m/s, 142 m^2/s, 0.3, 0.7), (0.017 m/s, 124 m^2/s, 0.3, 0.8), and (0.02 m/s, 117 m^2/s, 3.5, 5.2). Lower D_{KL} values indicate better agreement with the data.

in the seeding and partially absorbing cases is higher (about 28% and 41%, respectively) than in the fully reflecting and absorbing cases (about 12% and 5%, respectively) (Figure 4). The former are challenging scenarios that are sensitive to the choice of schemes for the boundary conditions in the random walk model. In this study, we chose specular reflection, the simplest and least accurate of these schemes for simplicity (Szymczak & Ladd, 2003).

An interesting nonphysical phenomenon that occurs when a free-passage solution is used to represent an absorbing boundary is the concept of "double counting." Due to the radiating boundary in the free-passage problem, at each time step, mass that would have otherwise been removed from the domain is retained and subsequently counted again at the next time step. This error compounds over time (Figure 3).

In all the cases considered in Figures 3 and 4, the discrepancies between the numerical solutions and equation (4) are due to the number of particles simulated in the random walk, the binning of the results of the random walk, and the finite difference approximation in equation (A2) in Appendix A.

4.2. Validation With Empirical Data

To demonstrate that our solution works well for practical applications, we compared the detections of tagged migrating fish in the San Joaquin River with the solutions given in equations (4) and (8) using the same parameter values for u and K in both cases. This is justified because the underlying system physics is identical in both cases, with only the boundary conditions being different. The values of u and K drop from 0.03 m/s and about 460 m^2/s for the first release group when the flow is high and ranges from 300 to 800 m^3/s to around 0.02 m/s and 120 m^2/s for the other release groups when the flow drops to approximately 200 m^3/s (Figure 5a).

Our solution performs considerably better than the free-passage solution when applied to the migrating fish (Figure 5). The free-passage solution estimates almost double the number of actual fish detections. This is an artifact of the phenomenon of double counting we discussed in section 4.1. Owing to the unobstructed passage of fish, the solution of equation (8) is also more dispersive than the solution of equation (4). In all releases, the Kulbeck-Leibler divergence between the solution in equation (4) and the detections at Station A3 is smaller than those with equation (8). Crucially, our solution is able to resolve important features such as the separation between the peaks of fish arrivals between the third and fourth release groups (Figures 5b and 5c).

5. Discussion

Our solution is able to recover both random walk results as well as observed detections of tagged fish in a real system with significantly better accuracy than commonly used approximate alternatives. In addition, typically used solutions by eigenfunction expansions (e.g., Golz & Dorroh, 2001; Smith, 1983) are cumbersome to apply for systems with nonradiating boundaries.

A significant advantage of equation (4) is scalability over both random walk simulations and continuum solution methods such as the finite volume approach. We note that our solution is recurrent and not in closed form; however, it can be rapidly computed numerically. Our solutions scales simply as tM on M spatial grid cells, as with vectorization the only operation involved is a matrix multiplication at each time step; the simplest Forward Euler random walk solutions scale as tN for N particles, typically with $N \gg M$; and the simplest continuum solutions scale as tM^2: The M^2 dependence is due to both a matrix inversion at each step in solving M coupled equations and severe time step size restrictions (see, e.g., Ferziger and Peric, 2012). Practically, we find that our solution is typically about 100 times faster than the 1-D numerical solution using a second-order accurate Crank-Nicolson scheme with central differencing on a spatial grid with 100 cells for large values of K. Moreover, on the order of 100,000 particles are needed to produce statistically reproducible particle tracking results, and so, our solution is typically about 1,000 times faster than a comparable simple particle tracking model. In this sense, equation (4) becomes extremely appealing for management applications.

Our solution is able to recover the qualitative characteristics corresponding to the different boundary types. For the fully reflecting boundary in Figure 4a, the gradient of the solution in equation (4) approaches 0, as expected for a no-flux boundary. For the fully absorbing boundary in Figure 4b, the solution in equation (4) is zero at the boundary. For the seeding and partially absorbing cases (Figures 4c and 4d), the solution approaches nonzero values corresponding to the flux at the boundary. Solutions such as equation (7) work under the approximations listed in section 1; however, they increasingly lose accuracy as the incipient mass nears the boundary. This is because the incipient flux is no longer similar to the free-passage flux (Figure 3). While it may seem practically appealing to neglect the boundary altogether and simply use the free-passage solution, the error propagated by that approximation increases from about 2% to more than 20% as the center of mass of the incipient mass nears the absorbing boundary (see Figure 2). As we reported in section 4.2, this is because of the double counting in the free-passage realization of the absorber of mass that should have been removed from the domain.

From an applications perspective, our solution of equation (4) is able to recover the general patterns in the first arrival times of fish migrating through the Delta. The double counting problem of expected numbers of fish passing the detector is effectively solved using the solution of equation (4). The agreement between predictions and data in this example highlights an important point about AD processes more generally: Even in cases where microscale processes are extremely complex, the 1-D-AD process may still provide an accurate approximation of dynamics on the appropriate time scale. In estuarine systems like the one in which the fish migration data were collected, changes in the hydrology due to storms, rainfall events, water extraction operations, and tides mean that system conditions are seldom stationary. Indeed, given the tidal nature of the flow in this system, as well as the time-varying swimming behavior of fish (e.g., Chapman et al., 2013), one might expect poor agreement between a simple 1-D-AD model and data. Nevertheless, the overall agreement between the predictions of equation (4) and data suggests that under relatively stationary conditions, the subtidal—or daily averaged—migration patterns of fish can be well represented by a simple advection-dispersion model with suitable boundary conditions, even in a complex tidal system.

6. Conclusion

We have developed a general solution to the 1-D-AD problem with streamwise boundaries. This solution can be applied to any type of boundary condition and is exact over the entire system domain, for all times, and for all Péclet number regimes. For real data, it also outperforms conventional approximate solutions. Moreover, it helps build the correct intuition about the physical process that the boundary continuously modifies the incipient density, rather than acting as a flux modifier to a free passage of mass. We have demonstrated that the approach recovers the density for the variety of boundary types that are possible. The real value of our solution method is its universal applicability to any type of boundary condition: One needs only vary α in

equation (4b) to recover the accurate solution for a given boundary value problem. Multiple boundaries such as channel junctions in stream networks or physical barriers to the flow or animal movement such as dams or fish screens can be readily incorporated using the superposition of suitably located images.

Practically, in fluid system applications with boundaries, the approximate solutions such as equation (7) or the free-passage solution in equation (8) perform poorly because they misrepresent the effect of the boundary for parts of the spatial domain close to the release location. We demonstrated an example in the study of acoustically tagged steelhead migrating through a section of the San Joaquin River. In this example our solution performs significantly better than conventional approximations.

The solution in equation (4) also serves as a guide for interpreting simulation results. Often, the results of particle tracking models are taken as is, and only their implications are analyzed subsequently (e.g., Kimmerer & Nobriga, 2008). Understanding what boundaries do to the incoming density will allow for more nuanced control of the systems themselves, when such control is desired. Because our solution handles any boundary type accurately over the entire system domain, at all times, and all Péclet number regimes, it is also an ideal tool to quickly examine real-world management alternatives before expending resources into more sophisticated models.

Appendix A: Numerical Solution Schemes

Here, we derive the various numerical approximations used in sections 3 and 5.

Second-Order Backward Difference Scheme

The solution by method of images in equation (4) in section 3.1 requires the numerical estimation of the density gradient at x_B. For accuracy, we chose the second-order backward difference formula given in (4c). This derived from the Taylor series expansion about x_B of $C(x_B - \Delta x, t)$ and $C(x_B - 2\Delta x, t)$ as

$$
\begin{aligned}
C(x_B - \Delta x, t) \quad &= C(x_B, t) - \left. \Delta x \frac{\partial C}{\partial x} \right|_{(x_B, t)} C(x_B - 2\Delta x, t) \\
&= C(x_B, t) - 2\Delta x \left. \frac{\partial C}{\partial x} \right|_{(x_B, t)} + \left. \frac{\Delta x^2 \partial^2 C}{2 \; \partial x^2} \right|_{(x_B, t)} - \text{H.O.T.} + 2\Delta x^2 \left. \frac{\partial^2 C}{\partial x^2} \right|_{(x_B, t)} - \text{H.O.T.}.
\end{aligned}
\tag{A1}
$$

Multiplying the first equation in (A1) by 4 and subtracting the second equation in (A1) from the resultant and rearranging gives, to second-order accuracy,

$$
\left. \frac{\partial C}{\partial x} \right|_{(x_B, t)} = \frac{3C(x_B, t) - 4C(x_B - \Delta x, t) + C(x_B - 2\Delta x, t)}{2\Delta x}.
\tag{A2}
$$

Numerical Implementation of Boundary Conditions

Here, we describe how to realize the different boundary conditions discussed in section 3.2 numerically. A seeding boundary can be realized numerically by both reflecting particles that have overshot the boundary, as well as by seeding new particles according to the mass balance at the boundary. The seeding flux at the boundary is a function of the arrival flux at the boundary. We now convert the densities to the number of particles by binning over a width $\frac{\Delta x}{2}$ adjacent to the boundary for accuracy. This gives in terms of the discrete equivalents of the densities

$$
N_{\text{In at } x_B}(t) = -\frac{v_B(t)\Delta t}{\Delta x / 2} N(x \geq x_B).
\tag{A3}
$$

These new particles will be seeded with a velocity of $v_B(t)$, thereby giving their position as

$$
x_p(n+1) = x_B + v_B(t)\Delta t.
\tag{A4}
$$

A partially absorbing boundary can be realized by noting that at the end of the domain, the absorption flux at the boundary is a function of the arrival flux at the boundary. This gives in terms of the discrete equivalents of the densities

$$N_{\text{Out at } x_B}(t) = \frac{v_B(t)\Delta t}{\Delta x / 2} N(x \geq x_B).$$

(A4)

In equation (A4), we use a bin width of $\frac{\Delta x}{2}$ for accuracy.

References

Bailey, N. T. (1952). Improvements in the interpretation of recapture data. *The Journal of Animal Ecology*, 21(1), 120–127. https://www.jstor.org/stable/1913

Banas, N. S., Hickey, B. M., MacCready, P., & Newton, J. A. (2004). Dynamics of Willapa Bay, Washington: A highly unsteady, partially mixed estuary. *Journal of Physical Oceanography*, 34(11), 2413–2427. https://doi.org/10.1175/JPO2637.1

Bennett, J. P. (1971). Convolution approach to the solution for the dissolved oxygen balance equation in a stream. *Water Resources Research*, 7(3), 580–590. https://doi.org/10.1029/WR007i003p00580

Berkowitz, B. (2002). Characterizing flow and transport in fractured geological media: A review. *Advances in water resources*, 25(8-12), 861–884. https://doi.org/10.1016/S0309-1708(02)00042-8

Brenner, H. (1962). The diffusion model of longitudinal mixing in beds of finite length. Numerical values. *Chemical Engineering Science*, 17(4), 229–243. https://doi.org/10.1016/0009-2509(62)85002-7

Burnham, K. P., & Anderson, D. R. (2002). *Model selection and multi-model inference*, 2nd Ed. *New York, NY: Springer-Verlag.*. https://doi.org/10.1007/b97636

Chapman, E. D., Hearn, A. R., Michel, C. J., Ammann, A. J., Lindley, S. T., Thomas, M. J., et al. (2013). Diel movements of out-migrating Chinook salmon (*Oncorhynchus tshawytscha*) and steelhead trout (*Oncorhynchus mykiss*) smolts in the Sacramento/San Joaquin watershed. *Environmental Biology of Fishes*, 96(2-3), 273–286. https://doi.org/10.1007/s10641-012-0001-x

Csiszár, I. (2003). Information projections revisited. *IEEE Transactions on Information Theory*, 49(6), 1474–1490. https://doi.org/10.1109/TIT.2003.810633

Danckwerts, P. V. (1953). Continuous flow systems. Distribution of residence times. *Chemical Engineering Science*, 50(24), 3857-3866. https://doi.org/10.1016/0009-2509(96)81811-2

Dimou, K. N., & Adams, E. E. (1993). A random-walk, particle tracking model for well-mixed estuaries and coastal waters. *Estuarine, Coastal and Shelf Science*, 37(1), 99–110. https://doi.org/10.1006/ecss.1993.1044

Ermak, D. L. (1977). An analytical model for air pollution transport and deposition from a point source. *Atmospheric Environment*, 11(3), 231–237. https://doi.org/10.1016/0004-6981(77)90140-8

Fischer, H. B., List, J. E., Koh, C. R., Imberger, J., & Brooks, N. H. (1979). *Mixing in inland and coastal waters*. San Diego, CA: Academic.

Golz, W. J., & Dorroh, J. R. (2001). The convection-diffusion equation for a finite domain with time varying boundaries. *Applied Mathematics Letters*, 14(8), 983–988. https://doi.org/10.1016/S0893-9659(01)00076-3

Grant, J., & Wilkinson, M. (2015). Advection–diffusion equation with absorbing boundary. *Journal of Statistical Physics*, 160(3), 622–635. https://doi.org/10.1007/s10955-015-1257-2

Gurney, W. S., Speirs, D. C., Wood, S. N., Clarke, E. D., & Heath, M. R. (2001). Simulating spatially and physiologically structured populations. *Journal of Animal Ecology*, 70(6), 881–894. https://doi-org.oca.ucsc.edu/10.1046/j.0021-8790.2001.00549.x

Kimmerer, W. J. (2008). Losses of Sacramento River Chinook salmon and delta smelt to entrainment in water diversions in the Sacramento–San Joaquin Delta. *San Francisco Estuary and Watershed Science*, 6(2). https://doi.org/10.15447/sfews.2008v6iss2art2

Kimmerer, W. J., & Nobriga, M. L. (2008). Investigating particle transport and fate in the Sacramento–San Joaquin Delta using a particle-tracking model. *San Francisco Estuary and Watershed Science*, 6(1). https://doi.org/10.15447/sfews.2008v6iss1art4

Kurylyk, B. L., & Irvine, D. J. (2016). Analytical solution and computer program (FAST) to estimate fluid fluxes from subsurface temperature profiles. *Water Resources Research*, 52, 725–733. https://doi-org.oca.ucsc.edu/10.1002/2015WR017990

LaBolle, E. M., Quastel, J., & Fogg, G. E. (1998). Diffusion theory for transport in porous media: Transition-probability densities of diffusion processes corresponding to advection-dispersion equations. *Water Resources Research*, 34(7), 1685–1693. https://doi-org.oca.ucsc.edu/10.1029/98WR00319

Lazarov, R. D., Mishev, I. D., & Vassilevski, P. S. (1996). Finite volume methods for convection-diffusion problems. *SIAM Journal on Numerical Analysis*, 33(1), 31–55. https://doi.org/10.1137/0733003

Lee, G. H., Friedrichs, C. T., & Vincent, C. E. (2002). Examination of diffusion versus advection dominated sediment suspension on the inner shelf under storm and swell conditions, Duck, North Carolina. *Journal of Geophysical Research Oceans*, 107(C7), 21–21. https://doi-org.oca.ucsc.edu/10.1029/2001JC000918

Loeck, J. F., Schramm, J., & Bodmann, B. E. J. (2018). On a model for pollutant dispersion in the atmosphere with partially reflective boundary conditions and data simulation using CALPUFF. *American Journal of Environmental Engineering*, 8, 112–117. https://doi.org/10.5923/j.ajee.20180804.05

Luce, C. H., Tonina, D., Gariglio, F., & Applebee, R. (2013). Solutions for the diurnally forced advection-diffusion equation to estimate bulk fluid velocity and diffusivity in streambeds from temperature time series. *Water Resources Research*, 49, 488–506. https://doi-org.oca.ucsc.edu/10.1029/2012WR012380

McEwan, D. R. (2001). Central valley steelhead. *Fish Bulletin*, 179(1), 1–43.

McKenzie, H. W., Lewis, M. A., & Merrill, E. H. (2009). First passage time analysis of animal movement and insights into the functional response. *Bulletin of Mathematical Biology*, 71(1), 107–129. https://doi.org/10.1007/s11538-008-9354-x

Monismith, S. G., Hench, J. L., Fong, D. A., Nidzieko, N. J., Fleenor, W. E., Doyle, L. P., & Schladow, S. G. (2009). Thermal variability in a tidal river. *Estuaries and Coasts*, 32(1), 100–110. https://doi.org/10.1007/s12237-008-9109-9

Moorcroft, P. R., & Lewis, M. A. (2006). *Mechanistic home range analysis (MPB-43). Monographs on Population Biology*. Princeton, NJ: Princeton University.

Moyle, P. B., Lund, J. R., Bennett, W. A., & Fleenor, W. E. (2010). Habitat variability and complexity in the upper San Francisco Estuary. *San Francisco Estuary and Watershed Science*, 8(3). https://doi.org/10.15447/sfews.2010v8iss3art1

Okubo, A., & Levin, S. A. (1989). A theoretical framework for data analysis of wind dispersal of seeds and pollen. *Ecology*, 70(2), 329–338. https://doi-org.oca.ucsc.edu/10.2307/1937537

Risken, H. (1996). *The Fokker-Planck equation*. Berlin, Germany: Springer.

Roberts, P. V., Reinhard, M., & Valocchi, A. J. (1982). Movement of organic contaminants in groundwater: Implications for water supply. *Journal of the American Water Works Association*, *74*(8), 408–413. https://doi-org.oca.ucsc.edu/10.1002/j.1551-8833.1982.tb04956.x

Rubbab, Q., Mirza, I. A., & Qureshi, M. Z. A. (2016). Analytical solutions to the fractional advection-diffusion equation with time-dependent pulses on the boundary. *AIP Advances*, *6*(7), 075318. https://doi.org.edu/10.1063/1.4960108

San Joaquin River Group Authority (2013). On implementation and Monitoring of the San Joaquin River Agreement and the Vernalis Adaptive Management Plan (VAMP). (2011 Annual Technical Report). Retrieved from http://www.sjrg.org/technicalreport/2011/2011_SJRGA_AnnualTechnicalReport.pdf

Schoellhamer, D. H. (2000). Influence of salinity, bottom topography, and tides on locations of estuarine turbidity maxima in northern San Francisco Bay. *Proceedings in Marine Science*, *3*, 343-357. https://doi.org/10.1016/S1568-2692(00)80130-8

Sibert, J. R., Hampton, J., Fournier, D. A., & Bills, P. J. (1999). An advection–diffusion–reaction model for the estimation of fish movement parameters from tagging data, with application to skipjack tuna (Katsuwonus pelamis). *Canadian Journal of Fisheries and Aquatic Sciences*, *56*(6), 925–938. https://doi.org/10.1139/f99-017

Smith, R. (1983). Effect of boundary absorption upon longitudinal dispersion in shear flows. *Journal of Fluid Mechanics*, *134*, 161–177. https://doi.org/10.1017/S0022112083003286

Speirs, D. C., & Gurney, W. S. (2001). Population persistence in rivers and estuaries. *Ecology*, *82*(5), 1219–1237. https://doi-org.oca.ucsc.edu/10.1890/0012-9658(2001)082[1219:PPIRAE]2.0.CO;2

Sridharan, V. K. (2015). *Scalar transport in channel networks: Development of a particle tracking model to study the movement of scalars in the Sacramento-San Joaquin Delta* (Doctoral dissertation). Retrieved from https://searchworks.stanford.edu/view/11384768. Stanford, CA: Stanford University.

Sridharan, V. K., Monismith, S. G., Fringer, O. B., & Fong, D. A. (2018). Evaluation of the delta simulation model-2 in computing tidally driven flows in the Sacramento-San Joaquin Delta. *San Francisco Estuary and Watershed Science*, *16*(2). https://doi.org/10.15447/sfews.2018v16iss2art6

Stockie, J. M. (2011). The mathematics of atmospheric dispersion modeling. *SIAM Review*, *53*(2), 349–372. https://doi-org.oca.ucsc.edu/10.1137/10080991X

Szymczak, P., & Ladd, A. J. C. (2003). Boundary conditions for stochastic solutions of the convection-diffusion equation. *Physical Review E*, *68*(3), 036704. https://doi.org/10.1103/PhysRevE.68.036704

van Genutchen, M. Th., & Alves, W. J. (1982). *Analytical solutions of the one-dimensional convective-dispersive solute transport equation*. (United States Department of Agriculture Technical Bulletin No. 1661). Retrieved from https://naldc.nal.usda.gov/download/CAT82780278/PDF

Visser, A. W. (1997). Using random walk models to simulate the vertical distribution of particles in a turbulent water column. *Marine Ecology Progress Series*, *158*, 275–281.

Wilkinson, M., Mehlig, B., & Gustavsson, K. (2010). Correlation dimension of inertial particles in random flows. *Europhysics Letters*, *89*(5), 50002. https://doi.org/10.1209/0295-5075/89/50002

Zabel, R. W., & Anderson, J. J. (1997). A model of the travel time of migrating juvenile salmon, with an application to Snake River spring chinook salmon. *North American Journal of Fisheries Management*, *17*(1), 93–100. https://doi.org/10.1577/1548-8675(1997)017<0093:AMOTTT>2.3.CO;2